

This is an open access article distributed under the terms of the Creative Commons Attribution 4.0 International License (CC BY 4.0), which permits use, distribution, and reproduction in any medium, provided the original publication is properly cited. No use, distribution or reproduction is permitted which does not comply with these terms.

# THERMOGRAPHIC MAPPING OF THE MELT POOL OF THE LASER POWDER BED FUSION PROCESS

Jiři Sika<sup>1</sup>, Vladimír Kindl<sup>2</sup>, Michal Křížek<sup>1</sup>, Tomáš Kavalíř<sup>1</sup>, Michal Frivaldský<sup>3,\*</sup>

- <sup>1</sup>Regional Technological Institute, Faculty of Mechanical Engineering, University of West Bohemia, Pilsen, Czech Republic
- <sup>2</sup>Regional Innovation Centre for Electrical Engineering, Faculty of Electrical Engineering, University of West Bohemia, Pilsen, Czech Republic
- <sup>3</sup>Department of Mechatronics and Electronics, Faculty of Electrical Engineering and Information Technologies, University of Zilina, Zilina, Slovakia

\*E-mail of corresponding author: michal.frivaldsky@feit.uniza.sk

 Vladimir Kindl © 0000-0003-2378-8059, Tomáš Kavalir © 0000-0002-3124-4986,

#### Resume

The article describes an advanced test stand for measuring temperatures during the 3D printing for additive manufacturing. Based on mathematical procedures, it analyzes the impact energy of the laser beam used in metal 3D printing.

The procedure is based on monitoring the flow of energy falling on the defined measuring object. Due to the design of this functional sample, it is also possible to analyze the incident and reflected energy to analyze and understand the physical properties, the precise quantitative distribution of temperatures, gradients, as well as the heating and cooling rates of the melt bath in laser bed fusion (L-PBF)

Available online: https://doi.org/10.26552/com.C.2023.065

# Article info

Received 13 April 2023 Accepted 28 June 2023 Online 12 July 2023

#### Keywords:

additive manufacturing 3D print laser measurement temperature thermo-camera

ISSN 1335-4205 (print version) ISSN 2585-7878 (online version)

#### 1 Introduction

It appears from globally available sources and a current trend, that additive manufacturing (AM) is gradually being used in mass production in the aerospace, automotive, health and jewelry industries. From such extensive use of AM, it might seem that it is already a standard and mastered production technology. However, production is primarily focused only on components that do not depend on the safety or operational reliability of assemblies [1].

Unfortunately, however, it is increasingly apparent that many basic questions are still unanswered. Additive technologies, thanks to their short history (30 years), are very little mapped in terms of the final characteristics of products and do not have uniform standards, procedures and safety risks developed for them, as is the case with conventional production methods. The need for improved quantitative understanding of the temperatures, gradients, as well as heating and cooling rates within

the melt pool in laser bed fusion (L-PBF), is widely known and studied. To address this need many studies has been initiated. A comprehensive summary of the available research in the field of additive technologies is collected in a paper initiated by the National Institute of Standards and Technology (NIST). Namely, the Measurement Science (MSAM) deals with measurement challenges concerning L-PBF and other metal Additive Manufacturing AM processes [2]. The principle of the Direct Metal Laser Sintering technology known in literature as DMLS is shown in the Figure 1.

Unlike the conventional materials, which are characterized by a polycrystalline microstructure formed by grains of different sizes and shapes, the microstructure of metallic AM products is typically cellular or dendritic and it is difficult to compare it to the structure of conventional materials. For AM products, the texture [3] produced by classical casting or forming of metals is not observed. The macrostructure of AM products differs significantly in the direction of printing

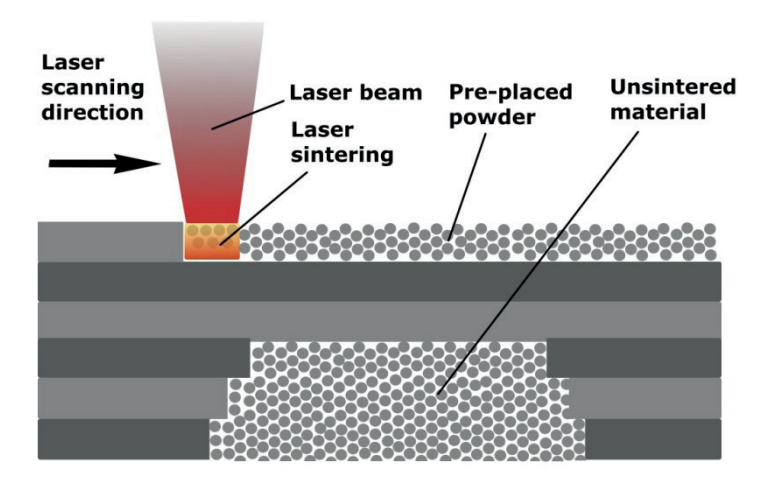


Figure 1 Principle of Direct Metal Laser Sintering (DMLS) technology

and in directions perpendicular to it. As a result, parts or test samples exhibit anisotropic mechanical properties when printed in the direction X, Y or Z, or at different angles of orientation and at different cross-sections of material thickness [4].

The strategy of the actual printing process includes the basic laser beam movements: contour movement and hatching. Hatching means that a metallic powder is sintered inside the part contour with a preset overlap between the partial movements of the laser, i.e. in its volume. In each layer, the angle of movement of the laser is subsequently changed. In addition, an overlap between the tracks is defined to ensure complete sintering in the entire volume of the component. This sintered material receives the final treatment by scanning the laser along the contour, which defines the respective cross-section. The final result also depends on whether the powder in one layer is sintered in only one direction or in perpendicular directions or alternating layers, etc. and on their combination, leading to the desired precision and surface roughness.

Based on this technology, defects are typically identified that affect repeatability, reliability, safety and, of course, mechanical properties, e.g. dynamic load, creep etc. Based on the new research, international standardization conditions that are focused on AM are constantly created and updated. However, this is very difficult because the AM process is affected by up to 50 parameters and inputs that are controlled by default, but some of them are difficult or almost impossible to control (e.g. powder size distribution, internal defects). Complex phenomena that occur during the melting, hardening and cooling of metallic powder (e.g. the direction and volume of the inert gas), impair the control of the sintering process. Current research is thus focused on optimizing or searching for the new methods, procedures, principles of solving inhomogeneity identified during the process and its elimination or minimization. Therefore, it is very important to have the input materials described in detail from the point of view of their structure and mechanical load, which the project aims to achieve with the 316L material.

There are several types of defects in metallic 3D printing [5], such as pores, cracks, residual stress and surface quality, which affect accuracy and stability. The tension in the material occurs during the melting process due to the rapid heating and cooling of the part. Significant manifestations of this phenomenon occur after the printing process. Therefore, it is important to be able to predict these states using numerical simulation. However, today's quality of calculations critically depends on the exact temperature field, which affects both residual stress and deformation. In work [6], the authors summarized the principles of voltage generation. As they state, it is still a combination of a high temperature gradient and fast cooling, which could be influenced by a special process or a different approach in the solution. They state that high residual tensile stress is very typical in the surface zone, while the presence of tension in the substrate is influenced by the total volume and construction of the part. Based on several experiments, they recommended several principles for stress minimization. Residual stress in metallic AM could be mitigated by in-process methods (e.g. preheating, process planning, feedback control, laser blasting) and post-process methods (e.g. machining and heat treatment, which is the most effective method for removing the residual stress). Another study was aimed at evaluating and predicting residual stress when changing heat (energy density) and layer thickness. Based on this, the layer thickness was optimized to improve the stress distribution. The main goal of the work [7] was to find the critical area and to eliminate stress-affected defects. The results were supported by a comparison between the FEM and practical results. An important conclusion that confirms the practical results is the possibility of reducing stress by more than 25 % when optimum layer thickness is used in the critical area and doubling the thermal input can reduce residual stresses by about 20 %.

| Table | , 1 | Thermocouples |
|-------|-----|---------------|
|       |     |               |

| Туре    | Material  |                | 3/                          | Accuracy                    |                          |
|---------|-----------|----------------|-----------------------------|-----------------------------|--------------------------|
|         | +         | -              | Measurement range           | Standard                    | Special                  |
| В       | Pt 30%-Rh | Pt 6%-Rh       | 870 - 1700 °C               | ± 0.5%                      | ± 0.25%                  |
| E Ni-Cr | Cu-Ni     | -270 - 0 °C    | ± 1.7% or ± 1.0%            | -                           |                          |
|         |           | 0 °C - 870 °C  | $\pm$ 1.7% or $\pm$ 0.5%    | $\pm$ 1.0% or $\pm$ 0.4%    |                          |
| J       | Fe        | Cu-Ni          | 0 - 760 °C                  | $\pm~2.2\%$ or $\pm~0.75\%$ |                          |
| K Ni-Cr | Ni-Al     | -200 - 0 °C    | $\pm$ 2.2% or $\pm$ 2.0%    | -                           |                          |
|         |           | 0 °C - 1200 °C | $\pm~2.2\%$ or $\pm~0.75\%$ | $\pm$ 1.1% or $\pm$ 0.4%    |                          |
| N       | Ni-Cr-Si  | Ni-Si-Mg       | 0 °C - 1260 °C              | $\pm~2.2\%$ or $\pm~0.75\%$ | $\pm$ 1.1% or $\pm$ 0.4% |
| R       | Pt 13%-Rh | Pt             | 0 °C - 1480 °C              | $\pm$ 1.5% or $\pm$ 0.25%   | $\pm$ 0.6% or $\pm$ 0.1% |
| S       | Pt 10%-Rh | Pt             | 0 °C - 1480 °C              | $\pm$ 1.5% or $\pm$ 0.25%   | $\pm$ 0.6% or $\pm$ 0.1% |
| T Cu    | Cu        | Cu-Ni          | -200 - 0 °C                 | $\pm$ 1.0% or $\pm$ 1.5%    | -                        |
|         | Cu-N1     | 0 °C - 370 °C  | $\pm$ 1.0% or $\pm$ 0.75%   | $\pm$ 0.5% or $\pm$ 0.4%    |                          |

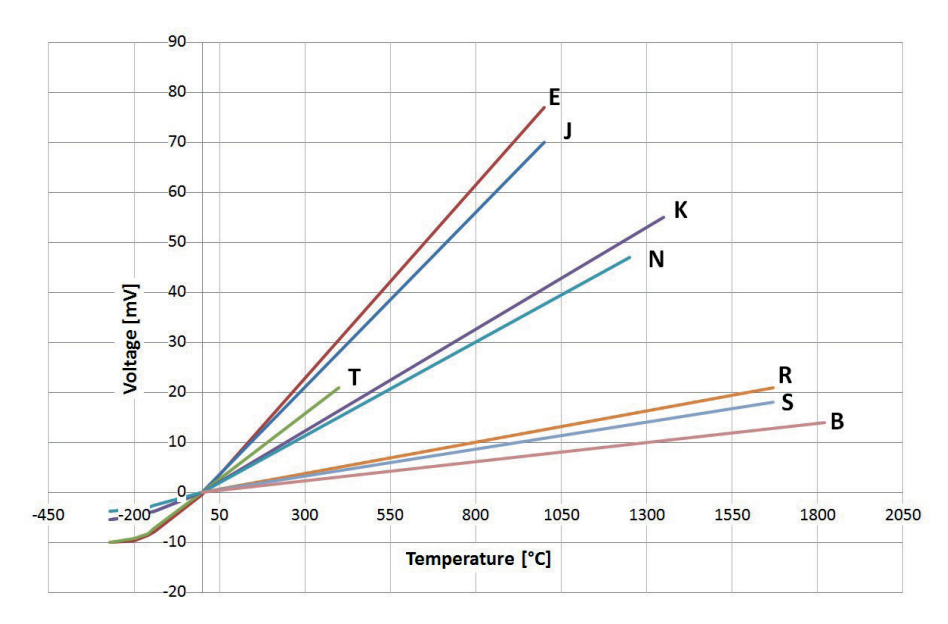


Figure 2 Thermocouple sensitivity as thermocouple voltage vs temperature for common thermocouple types, using a cold junction at  $0\,^{\circ}\mathrm{C}$ 

Among the more recent works related to the topic, it is worth mentioning the article [8] presents a method of measuring the thickness of powder layers during laser bed melting using in-situ infrared thermographic control. This technique provides a local and non-destructive approach to quality control in additive manufacturing processes. And the work [9-11] that maps melt pool dynamics within L-PBF technology.

# 2 Description of the job solution

The issue of using a thermal camera to monitor high temperatures, concerning the use of a fast thermal imager (photon principle) to measure the power and emissivity of the surface in additive 3D printing, by means of laser sintering, has been studied [12].

A stand for thermal imager measurement consisting

of the thermocamera FLIR SC-7500 equipped with f = 100 lens and a holder fixing the camera above a chamber view port has been compiled. The camera performs measurements simultaneously with the thermocouple, which measures the temperature directly on the measuring sample.

# 2.1 Direct thermocouple measurement

Direct Thermocouple Measurement - a survey of suitable thermocouples and their properties has been carried out (in terms of the maximum temperature range of measurement dynamics, etc.)

Non-insulated thermocouples have been selected and used and are ideal for applications where a quick response is required or where there is not enough space to store a standard thermocouple. The advantage is that

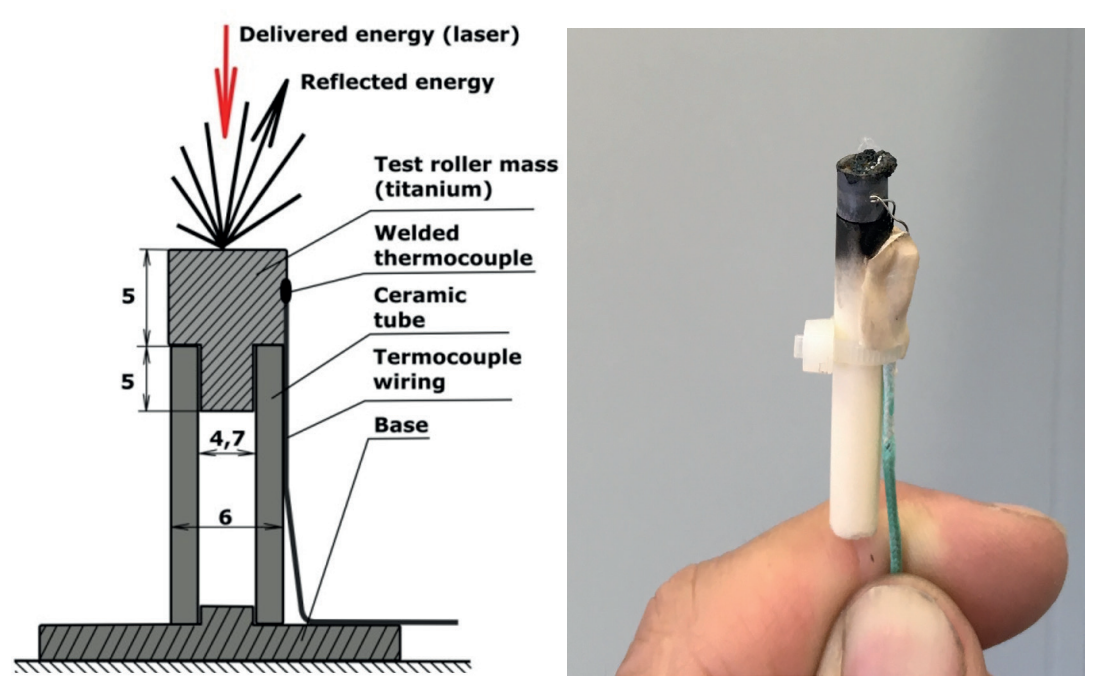


Figure 3 Setting of measuring titanium roller and prepared surface

the wire insulation materials cannot contaminate the process and have a quick response. They are available in thermocouples type K, T, J and E. Platinum/rhodium alloys are also available in thermocouples type R, S and B, Table 1.

The Figure 2 shows the relationship between temperature and voltage for various types of thermocouples.

To apply the new heat treatment processes with defined material structure and mechanical properties to 3D printing products, it was important to map the temperature field in the surface layer of the material in detail during the manufacturing process. The first experiments for detecting the thermal phenomena in the surface layer were based on the findings and default conditions from the device operator. First, the available measuring technology was specified.

Tests of direct temperature measurement on the surface of a defined titanium cylinder shape were performed (very small dimensions for good dynamic response and uniform heating of the entire volume in a short time with the help of laser supplied energy) and at the same time non-contact measurement was performed using a high-speed thermal imaging IR camera.

At the beginning, a thorough research was carried out in the field of the high-temperature contact measurements using thermocouples and a relatively less available thermocouple type B was chosen for measuring temperatures up to a range of around 1800 C°. Its advantage, in addition to the high limiting temperature, is also good linearity in the considered range, which is also related to the measurement accuracy. The disadvantage is the low thermoelectric voltage, especially in the lower thermal range, when this thermocouple is intended for measuring the lower

limit of temperatures up to approx. 200-300 C°. The conversion characteristics of the most commonly used thermocouples is shown in Figure 2. From the point of view of the material composition of the measuring roller, a titanium alloy with a melting point of up to around 1800 C° was chosen, which guarantees that it is possible to subsequently perform melting with the help of laser doping for common materials used in the field of additive manufacturing and to monitor their phase transformations during simultaneous measurement current temperature. The roller has a diameter of 6 mm and its design, together with a high-temperature ceramic support to minimize heat dissipation through the line, can be seen in Figure 3. The parameters of the test roller were: volume 228.2 mm<sup>3</sup>, weight: 0.001 [kg] and specific capacity of the material: 523 [J/kg/K].

# 2.2 Thermal imager

As mentioned above, during the contact measurements with the help of high-temperature thermocouples type B, a high-speed IR camera SC-7500 was used to display the temperature field. This measurement was chosen due to possible future calibration and the possibility of sensing and analyzing the temperature field only non-contact with the help of an IR camera. Since the thermocouple itself has order of magnitude higher measurement accuracy, it can then be used as a reference. The problem is the limited field of view through the small viewport in the hermetically sealed chamber of the additive printer (Figure 4) and the necessity to use the spectral filters (silicon glass) with additional attenuation, which, even after accounting for this attenuation, reduces the sensitivity of the system

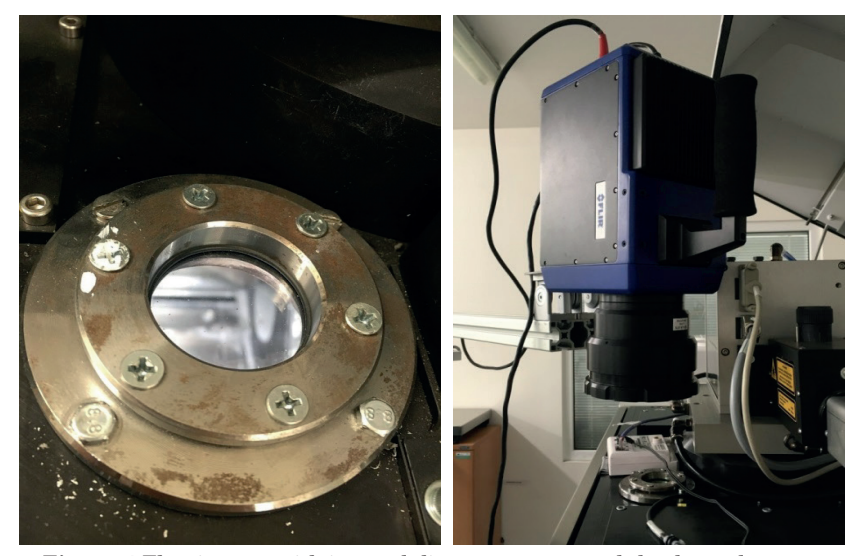


Figure 4 The viewport with internal diameter 30 mm and the thermal camera attached above the viewport of the 3D printer

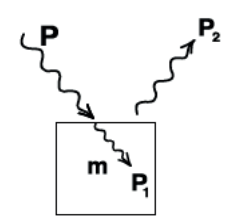


Figure 5 Power transfer for a body of mass m

and its overall accuracy. Some other features include the secondary viewport situated at the top of the printer that can include throughputs for thermocouple cabling. In Figure 4 is shown the location of the measuring highspeed camera above the window of the 3D printer itself.

# 3 Theoretical analysis of the thermal model

As a part of the experiment for indirect temperature measurement, tests of heating the test roller were carried out. The beam "hatched" the surface of the test roller for optimal and even energy transfer to the roller. Figure 5 shows the flow of heat energy relative to mass.

Subsequently, a theoretical analysis of the measured data was carried out in terms of temperature and power.

$$P = P_1 + P_2. (1)$$

Energy change P where  $P_1$  is the energy absorbed in the roller and  $P_2$  is the energy radiated

$$dw = m \cdot c \cdot dT. \tag{2}$$

dW represents the differential change in energy or work, measured in joules (J). It refers to the amount of energy transferred or work done. dT is a function of temperature and c represents the specific heat capacity

of the material, measured in joules per kilogram per Kelvin (J/kgK).

Then the energy change P is:

$$P = dW/dt, \ P = m \cdot c \cdot dT/dt, \tag{3}$$

the power received by the body to increase the temperature is then:

$$P_1 = m \cdot c \cdot dT_1/dt , \qquad (4)$$

while the time derivative of temperature is  $\frac{dT}{dt}$ .

The energy loss during the roller cooling is:

$$P_2 = m \cdot c \cdot dT_2/dt, \qquad (5)$$

for T near the intersection of  $T_1$  and  $T_2$ , the losses  $P_2$  [W] and the power received by the body during the heating  $P_1$  without losses are determined, Figures 6 and 7.

### 4 Experimental measurement

The aim was to set the measurement methodology to be suitable to the EOS M290 commercial L-PBF system. The same measurement methodology has always been

followed, where the laser power on the machine was gradually adjusted to levels from 50 W to 350 W. The beam "hatched" the surface of the test roller for optimal and even transfer of energy to the roller. Subsequently, the power-to-temperature ratio was evaluated as the main output.

### 4.1 Emissivity

To convert a measured camera signal into a true temperature, the surface emissivity must be known. There are multiple methods for measuring emissivity. [13] notes several methods for calculating emissivity measurement uncertainty. The emissivity of titanium roller depends on various factors such as surface finish, temperature, and wavelength of radiation. Titanium has a relatively low emissivity. Polished or oxidized titanium surfaces typically have emissivity values ranging from

0.1 to 0.7. However in some cases, if the surface is rough or coated, the emissivity can be higher. The test titanium roller has its surface very rough, therefore the emissivity value on the camera was set to 1, the influence of the attenuation of the spectral filter has not yet been considered.

#### 4.2 Measurement results and calculation

All the thermocouple measurements of temperature and data from IR camera are shown in Figures 8 to 11 depending on laser power. The maximum value represents the highest temperature recorded within the measured area and indicates the hottest point or object in the field of view. The mean value represents the average temperature calculated by summing up all the temperature values within the measured area.

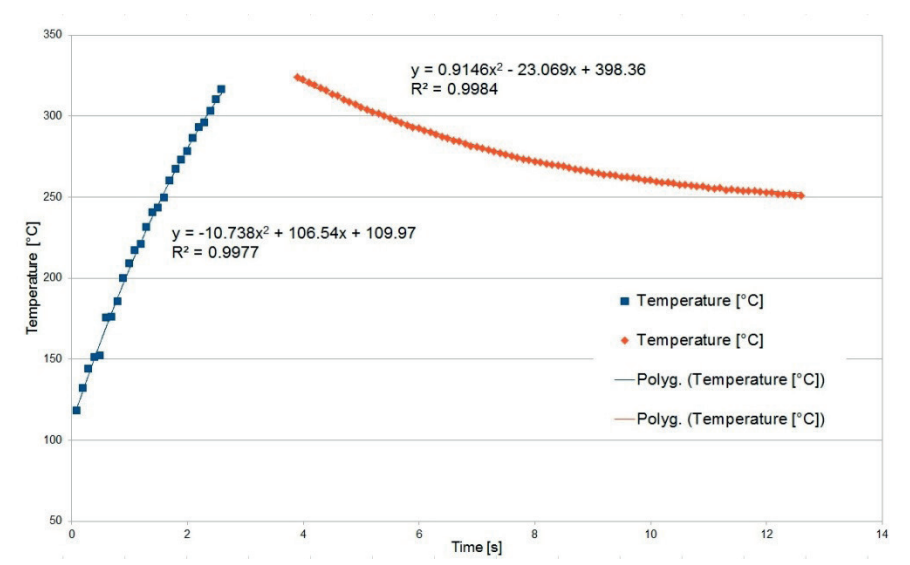


Figure 6 Heating and cooling temperature measured data at a laser beam power level of 50W

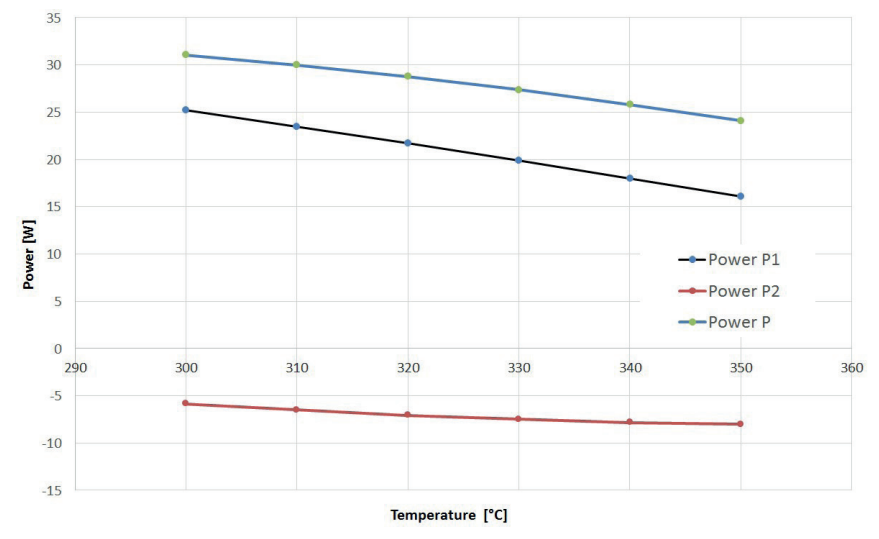


Figure 7 Calculated power at a laser beam power level of 50W

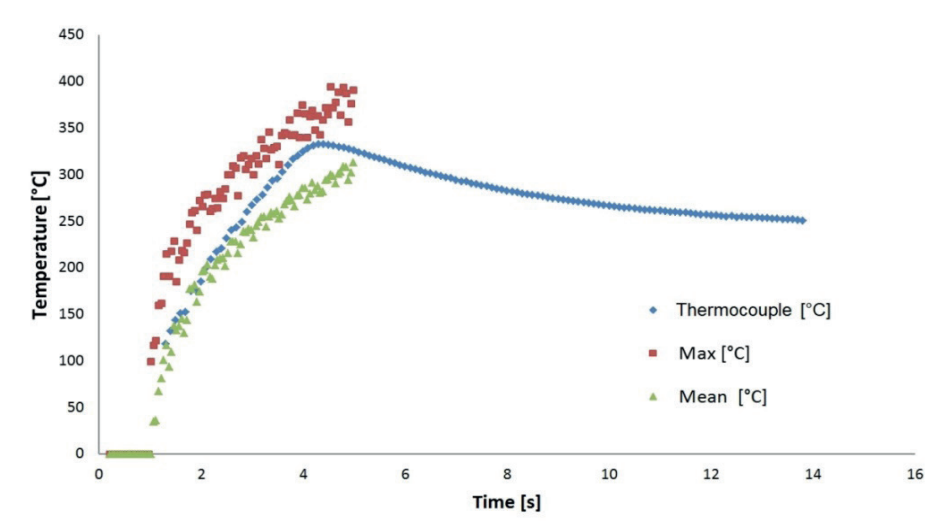
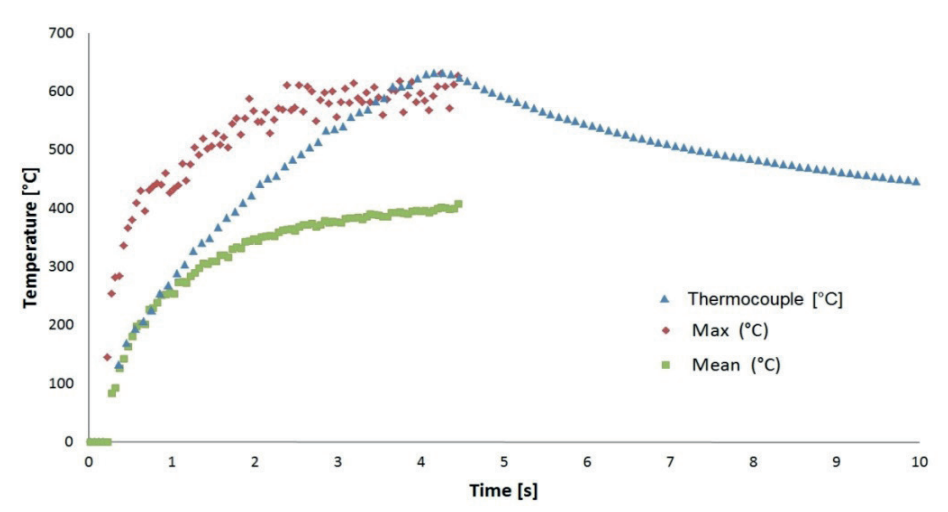


Figure 8 Relationship between the thermocouple and IR camera for 50 W of laser power



 $\it Figure~9~Relationship~between~the~thermocouple~and~IR~camera~for~100~W~of~laser~power$ 

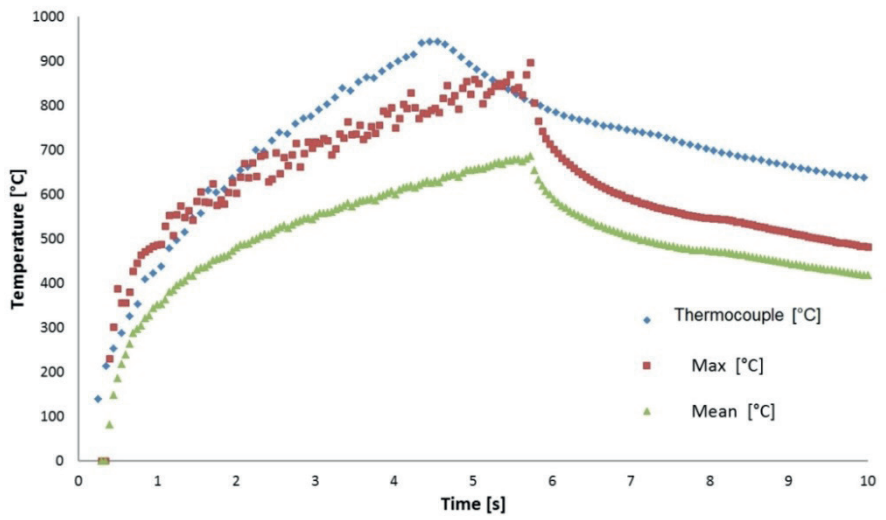


Figure 10 Relationship between the thermocouple and IR camera for 150 W of laser power

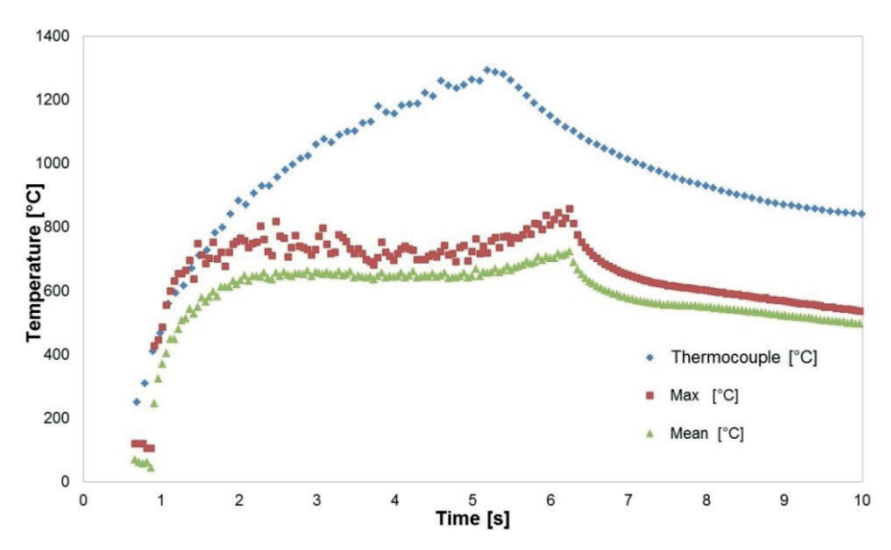


Figure 11 Relationship between the thermocouple and IR camera for 300 W of laser power

#### 5 Discussion

The thermal imaging experiments of the heat process were performed while maintaining the same rendering time and path, at seven power levels (50, 100, 150, 200, 250, 300, and 350 W) of the commercial EOS 270M L-PBF machine.

A special B-type (Pt-Rh) thermocouple enabling the high measurement dynamics and measuring temperatures in the range of 870 to 1700 °C, placed (spot-welded on the surface) on a titanium roller, was used to measure the increase in temperature, which was in time correlation with the supplied energy.

At the same time, a FLIR SC-7500 high-speed thermal camera, with an external filter and calibration in the thermal range of 300 to 1500 degrees, was used. With the help of this camera, the irradiated surface of the measuring roller was scanned and its temperature was evaluated from the resulting video sequence.

There was a noticeable agreement between the measurement recorded by the IR camera and the real measurement using the thermocouple, i.e. the temperature increase depending on the supplied energy by the laser beam was determined by calculation and this was compared to the real measurement.

The measurement agreement between the thermocouple and the thermocamera was for values of 50, 100, 150 W of laser power. For higher values, the measurement values from the high-speed thermocamera were significantly lower than those of the reference thermocouple. The use of IR thermal vision at higher incident energies (LASER power higher than approx. 250 W) is problematic due to the divergence between the contact measurement using a thermocouple and non-contact measurement using an IR high-speed thermal camera. It is seen on

the graph in Figure 8. This was probably caused by formation of a plasma cloud, which is caused by the too high impact energy of the laser beam. The mentioned plasma cloud then probably behaves as a spectral filter in the IR region.

#### 6 Conclusion

In this research, the objective was to investigate the power delivered by a laser beam during metal 3D printing using the laser bed fusion method. The study focused on a specific mass in the form of a titanium roller, with the laser power on the machine gradually adjusted from 50 W to 350 W. By the end of the research, the measured data obtained through the calculation procedure confirmed the declared power supplied by the device to the titanium cylinder. This finding signifies the accuracy and reliability of the laser power settings on the machine, ensuring that the intended power levels were effectively delivered during the 3D printing process. The successful confirmation of the power supplied to the titanium roller enhances the understanding and control of the metal 3D printing process, providing valuable insights for optimizing parameters and achieving desired outcomes in similar applications.

#### Acknowledgment

This contribution has been prepared within the project ITI CZ.02.1.01/0.0/0.0/18\_069/0010040, "Research of additive technologies for future application in mechanical engineering practice-RTI plus" under the auspices of the National Sustainability Programme

I of the Ministry of Education, Youth and Sports of the Czech Republic aimed at supporting research, experimental development and innovation and within the project OP VVV Electrical Engineering Technologies with High-Level of Embedded Intelligence CZ.02.1.01/0. 0/0.0/18 069/0009855.

#### **Conflicts of interest**

The authors declare that they have no known competing financial interests or personal relationships that could have appeared to influence the work reported in this paper.

### References

- [1] MANI, M., LANE, B., DONMEY, M. A., FENG, S., MOZLAN, S., FESPERMEN, R. Measurement science needs for real-time control of additive manufacturing powder bed fusion process [online]. NIST Internal Report (NISTIR) 8036. Gaithersburg, MD, USA: National Institute of Standards and Technology, 2015. Available from: https://doi.org/10.6028/NIST.IR.8036
- [2] LANE, B. M., MOLYAN, S. P., WHITEON, E. P., MA, L. Thermographic measurements of the commercial laser powder bed fusion process at NIST. *Rapid Prototyping Journal* [online]. 2016, 22(5), p. 778-787. ISSN 1355-2546. Available from: https://doi.org/10.1108/RPJ-11-2015-0161
- [3] SURYAWANSHI, J., PRASHANTH, K. G., RAMAMURTY, U. Tensile, fracture and fatigue crack growth properties of a 3D printed maraging steel through selective laser melting. *Journal of Alloys and Compounds* [online]. 2017, 725, p. 355-364. ISSN 0925-8388, eISSN 1873-4669. Available from: https://doi.org/10.1016/j. jallcom.2017.07.177
- [4] MONKOVA, K., ZETKOVA, I., KUCEROVA, L., ZETEK, M., MONKA, P., DANA, M. Study of 3D printing direction and effects of heat treatment on mechanical properties of MS1 maraging steel. Archive of Applied Mechanics [online]. 2019, 89, p. 791-804. ISSN 0939-1533, eISSN 1432-0681. Available from: https://doi.org/10.1007/s00419-018-1389-3
- [5] TAMMAS-WILLIAMS, S., ZHAO, H., LEONARD, F., DERGUTI, F., TODD, I., PRANGNELL, P. B. XCT analysis of the influence of melt strategies on defect population in Ti-6Al-4V components manufactured by selective electron beam melting. *Material Characterization* [online]. 2015, 102, p. 47-61. ISSN 1044-5803, eISSN 1873-4189. Available from: https://doi.org/10.1016/j.matchar.2015.02.008
- [6] LI, C., LIU, Z. Y., FANG X. Y., GUO, Y. B. Residual stress in metal additive manufacturing. *Procedia CIRP* [online]. 2018, 71, p. 348-353. eISSN 2212-8271. Available from: https://doi.org/10.1016/j.procir.2018.05.039
- [7] MUKHERJEE, T. ZHANG, W, DEBROY, T. An improved prediction of residual stresses and distortion in additive manufacturing. *Computational Materials Science* [online]. 2017, **126**, p. 360-372. ISSN 0927-0256, eISSN 1879-0801. Available from: https://doi.org/10.1016/j.commatsci.2016.10.003
- [8] LIU, T., LOUGH, C. S., SEHHAT, H., REN, Y. M., CHRISTOFIDES P. D., KINZEL, E.C., LEU, M. C. In-situ infrared thermographic inspection for local powder layer thickness measurement in laser powder bed fusion. Additive Manufacturing [online]. 2022, 55, 102873. ISSN 2214-8604, eISSN 2214-7810. Available from: https://doi.org/10.1016/j.addma.2022.102873
- [9] REHMAN, A. U. PITIR, F., SALAMCI, M. U. Full-field mapping and flow quantification of melt pool dynamics in laser powder bed fusion of SS316L. *Materials* [online]. 2021, 14(21), 6264. eISSN 1996-1944. Available from: https://doi.org/10.3390/ma14216264
- [10] ZHENG, L., ZHANG, Q., CAO, H., WU, W., MA, H., DING, X., YANG, J., DUAN, X., FAN, S. Melt pool boundary extraction and its width prediction from infrared images in selective laser melting. *Materials and Design* [online]. 2019, 183, 108110. ISSN 0264-1275, eISSN 1873-4197. Available from: https://doi.org/10.1016/j. matdes.2019.108110
- [11] OBEIDI, M. A., AHAD I. A., BRABAZON, D. Investigating the melt-pool temperature evolution in laser-powder bed fusion by means of infra-red light: a review. *Key Engineering Materials* [online]. 2022, **926**, p. 235-241. ISSN 1662-9795. Available from: https://doi.org/10.4028/p-6fn67z
- [12] BAYLE, F., DOUBENSKAIA, M. Selective laser melting process monitoring with high speed infra-red camera and pyrometer. In: Fundamentals of Laser Assisted Micro- and Nanotechnologies, 2007: proceedings [online]. SPIE. Vol. 6985. 2008. Available from: https://doi.org/10.1117/12.786940
- [13] MADDING, R. P. Emissivity measurement and temperature correction accuracy considerations. In: AeroSense '99: proceedings [online]. SPIE. Vol. 3700 Thermosense XXI. 1999. Available from: https://doi.org/10.1117/12.342307